RSC
Medicinal Chemistry

ROYAL SOCIETY OF CHEMISTRY

RESEARCH ARTICLE

View Article Online
View Journal | View Issue

Cite this: *RSC Med. Chem.*, 2023, **14**, 934

Identification of ARUK2002821 as an isoform-selective PI5P4Kα inhibitor†

Henriëtte M. G. Willems, Simon Edwards, Helen K. Boffey, Stephen J. Chawner, Christopher Green, ‡ Tamara Romero,‡ David Winpenny, John Skidmore, Jonathan H. Clarke and Stephen P. Andrews *

Received 24th January 2023,
Accepted 3rd April 2023

DOI: 10.1039/d3md00039g

rsc.li/medchem

The phosphatidylinositol 5-phosphate 4-kinases (PI5P4Ks) play a central role in regulating cell signalling pathways and, as such, have become therapeutic targets for diseases such as cancer, neurodegeneration and immunological disorders. Many of the PI5P4Kα inhibitors that have been reported to date have suffered from poor selectivity and/or potency and the availability of better tool molecules would facilitate biological exploration. Herein we report a novel PI5P4Kα inhibitor chemotype that was identified through virtual screening. The series was optimised to deliver ARUK2002821 (**36**), a potent PI5P4Kα inhibitor (pIC_{50} = 8.0) which is selective *vs.* other PI5P4K isoforms and has broad selectivity against lipid and protein kinases. ADMET and target engagement data are provided for this tool molecule and others in the series, as well as an X-ray structure of **36** solved in complex with its PI5P4Kα target.

Introduction

Phosphatidylinositol and the phosphorylated derivatives of this amphiphilic membrane phospholipid have integral roles in many cellular processes that are mediated through cell signalling and control of membrane dynamics.[1] Phosphoinositide species are defined by the accumulation of phosphate groups onto the cyclic *myo*-inositol ring that constitutes the accessible hydrophilic headgroup when the lipid is integrated into a cellular membrane. The seven discovered phosphoinositide species (phosphorylated on positions 3–5 of the 6-carbon ring of this phosphatidylinositol headgroup) have been suggested to have mediator roles in a wide variety of cellular metabolic processes such as channel regulation, membrane trafficking, proliferation and cell death/stress responses such as autophagy and apoptosis.[1–4] As a consequence, the roles of phosphoinositides in human diseases have received much recent attention and are well documented in developmental disorders (including channelopathies and ciliopathy syndromes), neurodegeneration and cancer.[5–9]

Mammals express three isoforms (α, β and γ) of phosphatidylinositol 5-phosphate 4-kinases (PI5P4Ks), the enzymes that generate phosphatidylinositol bisphosphate (PIP_2) from phosphatidylinositol phosphate (PIP), principally *via* the conversion of PI(5)*P* to PI(4,5)P_2. Variation in catalytic site and putative G-loop sequences may account for the large differences in intrinsic *in vitro* kinase activity between the isoforms (PI5P4Kα being the most active isoform).[10] The PI5P4Ks have established links to cancer,[9,11] specific associations suggest that inhibition of PI5P4Kα may be beneficial in p53 mutant breast cancer[12,13] and acute myeloid leukaemia[14] where *PIP4K2A* has been identified as a cytogenetic risk factor.[15,16] This association potentially reflects the role of PI5P4Kα in cell proliferation and the higher levels of expression in hematopoietic cells.[17]

Various PI5P4K inhibitors have been reported to have a therapeutic effect in oncology settings.[18,19] Covalent pan-PI5P4K inhibitor THZ-P1-2 (**1**) was shown to have anti-proliferative activity in acute myeloid and lymphoblastic leukaemias (AML/ALL)[19–22] and the small molecule A131 (**2**), which was shown to target mitotic pathways and PI5P4Ks, was effective in cancer cell-specific lethality[18] (Fig. 1). Compound CC260 (**3**), with dual activity at PI5P4Kα and PI5P4Kβ,[13] reduced proliferation in p53 null cancer cell lines in the presence of stress caused by nutrient depletion, in concordance with earlier findings.[12] More specifically, selective inhibition of PI5P4Kα may also have positive therapeutic effects, as demonstrated by the genetic depletion of PI5P4Kα in p53 null THP-1 cells which resulted in the inhibition of proliferation and also prevented AML development in xenografts.[14]

The ALBORADA Drug Discovery Institute, University of Cambridge, Island Research Building, Cambridge Biomedical Campus, Hills Road, Cambridge, CB2 0AH, UK. E-mail: spa26@cam.ac.uk

† Electronic supplementary information (ESI) available. CCDC 2237386 and 2237387. For ESI and crystallographic data in CIF or other electronic format see DOI: https://doi.org/10.1039/d3md00039g

‡ Christopher Green and Tamara Romero: UK Dementia Research Institute, University of Cambridge, Island Research Building, Cambridge Biomedical Campus, Hills Road, Cambridge, CB2 0AH, UK.

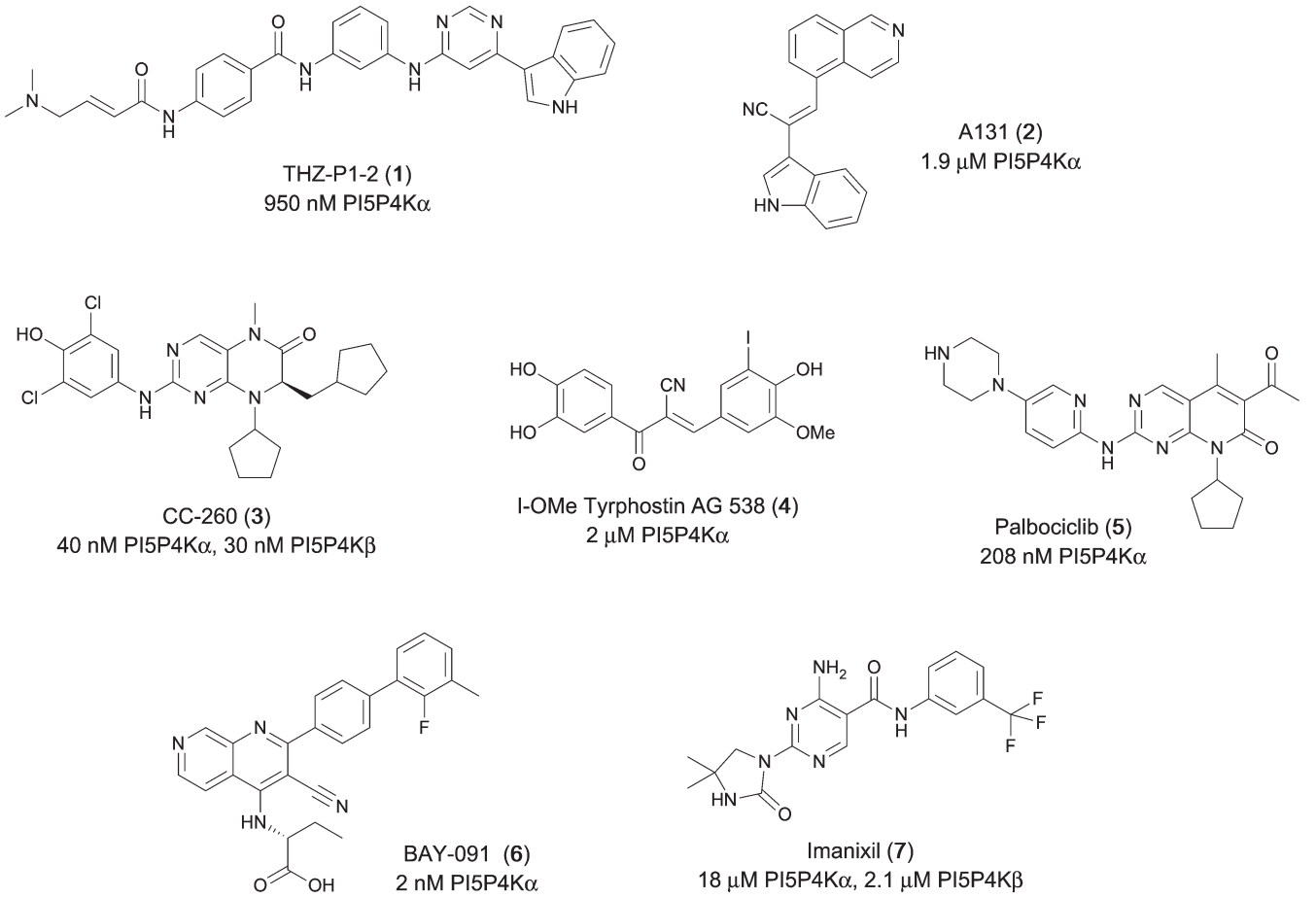

Fig. 1 Published PI5P4Kα inhibitors with their reported activity values.

There have been other reports of small molecule PI5P4Kα inhibitors, such as the tyrphostins, with I-OMe-tyrphostin AG538 (**4**) having the highest reported activity.[23] The CDK4/6 inhibitor, palbociclib (**5**) has also been reported to be a PI5P4Kα inhibitor,[24] however, this compound was found to be inactive in ADP-Glo assays for all 3 isoforms of PI5P4K in our laboratory.[25] BAY-091 (**6**) was recently identified as a selective PI5P4Kα chemical probe following HTS of 3.9 million compounds at Bayer[26] but the compound did not show anti-proliferative activity in p53-null cells. Imanixil (**7**) was developed by Sanofi-Aventis who subsequently characterised it as a PI5P4Kβ inhibitor with some PI5P4Kα activity.[27]

Results

As part of our investigations we were interested in identifying inhibitors for each of the PI5P4K isoforms, α, β and γ. We have previously described efforts to improve the PI5P4Kγ inhibitor, NIH12848,[28] and a virtual screening approach to identify novel PI5P4Kγ inhibitors.[25] Owing to the high sequence similarity between the PI5P4K isoforms, a single virtual screening approach was adopted for PI5P4Kα and PI5P4Kγ.[25] To identify biologically-active PI5P4Kα inhibitors, the 960 virtual screening hits previously described were screened in an ADP-Glo kinase functional assay using **4** as a positive control. This identified 9 compounds with pIC_{50}s > 5 against PI5P4Kα, which are shown in Table 1. From this set, **8** had the highest activity (pIC_{50} = 6.4) and had an active near neighbour (**9**).

These hits were followed up with analogue purchases where possible, with compounds being selected by substructure, Tanimoto similarity or shape similarity. In total, 60 analogues were purchased for **10**, but only two were weakly active (Table S1†), and 42 analogues of **11** were purchased, 2 of which showed pIC_{50}s > 5, but none were more potent than **11** (Table S2†). None of the 24 analogues purchased for the **12**/**13**/**14** cluster showed activity and no suitable commercial analogues of **15** or **16** were identified. In contrast, several purchased analogues of the **8** series showed PI5P4Kα activity, with two showing increased potency. This series was therefore selected for further optimisation. PI5P4Kα and PI5P4Kγ+ data for all purchased analogues of **8** is available in ESI† (Table S3).

To further probe the utility of compound **7** as a hit for development, the compound was synthesised then screened in-house using previously described ADP-Glo assays for PI5P4Kα, β and γ+.[28] The compound was found to be inactive

Table 1 PI5P4Kα and PI5P4Kγ+ pIC_{50}s of the top virtual screening hits

		Inhibition of PI5P4K (ADP-Glo)			Physicochemical properties	
		PI5P4Kα pIC_{50}	PI5P4Kα LE	PI5P4Kγ+ pIC_{50}	MW	*X* log *P*
8	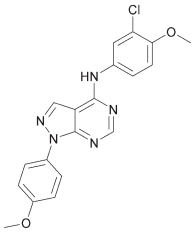	6.4	0.33	4.9	382	4.2
9	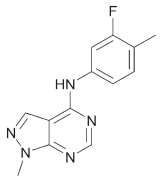	5.2	0.38	<4.3	257	2.4
10	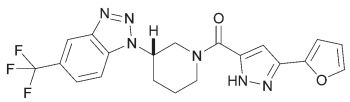	5.7	0.26	ND	430	4.6
11	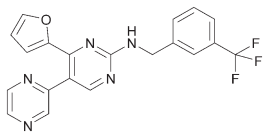	5.4	0.26	4.9	397	3.4
12	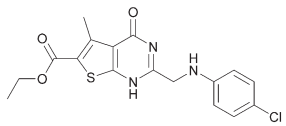	5.1	0.28	<4.3	378	3.8
13	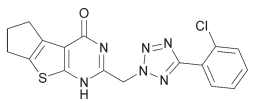	5.6	0.30	4.8	385	3.5
14	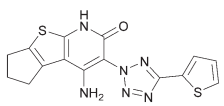	5.4	0.32	4.7	356	2.5
15	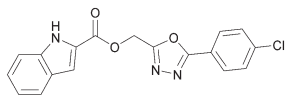	5.3	0.30	<4.3	354	5.5
16	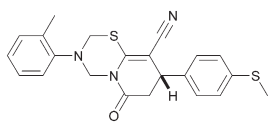	5.5	0.27	<4.3	408	5.4

in all cases in our hands. The chemical structure was verified by NMR, LCMS and small molecule X-ray crystallographic analysis and found to be consistent with the reported structure.[27] Further, compound **7** was screened externally against two commercially-available lipid kinase assay panels and was found to have essentially no activity (see ESI† Tables S4–S9 for further details on the screening and small molecule X-ray crystal structure). This chemotype was not pursued for further development.

Analogues of **8** were purchased or synthesised then screened against PI5P4Kα in iterations in order to understand the SAR of the series, with PI5P4Kγ+ being used as a control for isoform selectivity (Table 2). In general, this chemotype showed little or no measurable inhibition of PI5P4Kγ+ activity. Lipophilic substituents on both aryl rings, R^1 and R^2, were generally preferred for PI5P4Kα activity and aryl group R^2 showed a preference for a lipophilic substituent at position 4 of the ring, such as methoxy (**8**) or methyl (**17**) *vs.* unsubstituted (**18**). An electron-withdrawing chloro group at the 4-position did not work well (**19**) unless combined with a substituent at the 2-position (**20**) which is postulated to induce a conformational twist, as discussed in further detail

Table 2 SAR exploration at positions R^1 and R^2

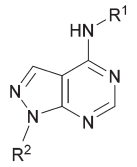

	R^1	R^2	Inhibition of PI5P4K (ADP-Glo) PI5P4Kα pIC_{50}	PI5P4Kα LE	PI5P4Kγ+ pIC_{50}	Physicochemical properties MW	*X* log *P*
8	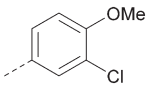	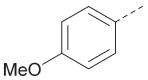	6.4	0.33	4.9	382	4.2
17	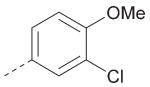	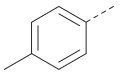	6.9	0.37	<4.3	366	4.5
18	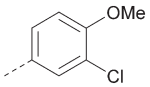		5.9	0.33	<4.3	352	4.2
19	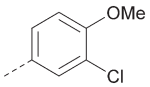	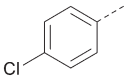	<4.3	NA	<4.9	386	4.8
20	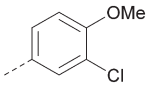	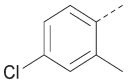	6.6	0.34	<4.6	400	5.1
21	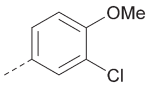	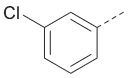	<4.7	NA	<4.3	386	4.8
22	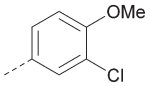	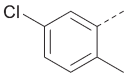	5.6	0.29	<4.5	400	5.1
23	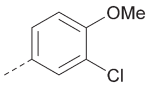	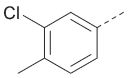	<4.3	NA	<4.3	400	5.1
24	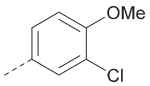	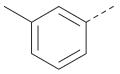	6.3	0.34	<4.3	366	4.5
25	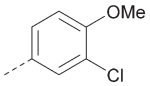	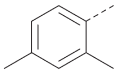	7.0	0.36	<4.3	380	4.8
26	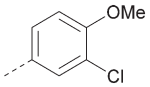	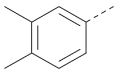	7.1	0.37	<4.3	380	4.8
27	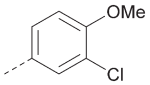	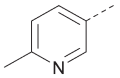	5.7	0.31	<4.3	367	3.1
28	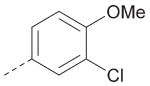	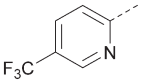	<4.3	NA	<4.3	421	4.3
29	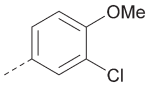		<4.6	NA	<4.7	316	3.2
30		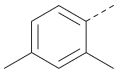	4.8	0.25	<4.2	281	3.4
31	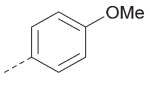	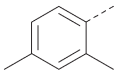	5.9	0.32	<4.3	345	4.2
32	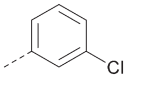	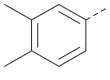	<4.3	0.24	<4.3	350	4.8

Table 2 *(continued)*

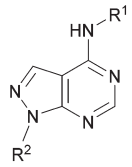

	R^1	R^2	Inhibition of PI5P4K (ADP-Glo) PI5P4Kα pIC_{50}	PI5P4Kα LE	PI5P4Kγ+ pIC_{50}	Physicochemical properties MW	*X* log *P*
33	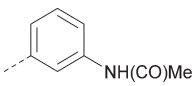	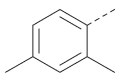	5.9	0.30	<4.7	372	3.9
34	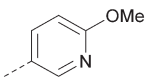	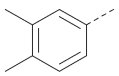	6.5	0.35	<4.3	346	3.3
35	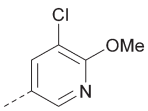	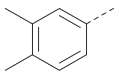	<4.3	0.22	<4.3	381	3.9

Table 3 Variation of the core

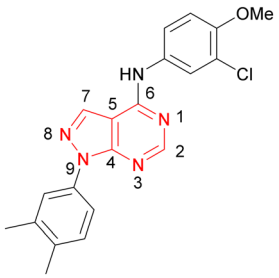

	Inhibition of PI5P4K (ADP-Glo) PI5P4Kα pIC_{50}	PI5P4Kα LE	PI5P4Kγ+ pIC_{50}	Physicochemical properties MW	*X* log *P*
26	7.1	0.37	<4.7	380	4.8
36	8.0	0.42	<4.3	379	5.8
37	<4.6	NA	<4.4	378	6.3
38	<4.3	NA	<4.5	378	6.0
39	6.9	0.35	<4.6	395	4.9
40	<4.3	NA	<4.3	393	6.1

below. Similarly, chloro was not tolerated at the 3-position (**21**) unless there was an *ortho* substituent to elicit the conformational twist (compare **22** with a para group in **23**). Conversely, an electron-donating methyl group was tolerated at position 3 or 4 without a conformational lock (**24** and **17**). These subtle differences in chloro *vs.* methyl are discussed in detail below. The combination of 4-methyl with a second substituent worked well in the cases of **25** and **26.** There were early indications that an aromatic heterocycle may be tolerated at position R^2 in some cases (compare **27** and **28**) but replacing this aryl group with a small aliphatic group ablated activity (**29**). A small lipophilic group was not tolerated at position R^1 (**30**) and deletion of the 3-Cl or 4-OMe from the R^1 aryl ring caused a significant drop in activity (compare **31** with **25** and **32** with **26**). It was desirable to introduce a more polar substituent on the R^1 aryl ring or heteroatoms within the ring to modulate physicochemical properties and early attempts to do so suggested this might be possible with the correct combination and orientation of substituents (compare **33**, **34** and **35**).

A number of analogues with variations to the bicyclic core was synthesised whilst keeping the R^1 and R^2 substituents fixed to provide matched pairs with **26** (Table 3). Replacement of the ring N by CH at position 8, to generate a pyrrolopyrimidine, proved the most successful strategy for increasing binding affinity and cell potency (**36**) whereas replacement of the ring N by CH at positions 1 or 3 led to complete loss of activity (**37** and **38**). The pyrrolopyrimidinone derivative, **39**, showed a marked reduction in $X\log P$ compared to **36** and was equipotent to compound **26.** Methylation at the 7-position was not tolerated (**40**).

Using the pyrrolopyrimidine template of **36** as a new lead, further analogues were synthesised. As with **25** *vs.* **26**, 2,4-dimethylphenyl on the pyrrolopyrimidine core was

Table 4 SAR for varying R^1 and R^2 on the pyrrolopyrimidine core

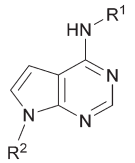

	R^1	R^2	Inhibition of PI5P4K (ADP-Glo)			Physicochemical properties	
			PI5P4Kα pIC_{50}	PI5P4Kα LE	PI5P4Kγ+ pIC_{50}	MW	$X\log P$
36	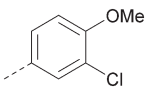	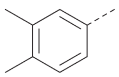	8.0	0.42	4.3	379	5.8
41	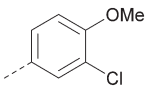	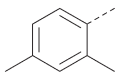	7.7	0.40	<4.5	379	5.8
42	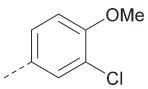	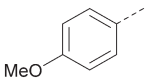	7.4	0.39	<4.5	381	5.2
43	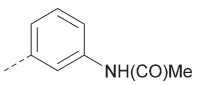	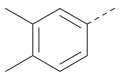	6.8	0.34	4.5	371	4.9
44	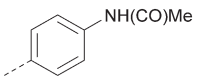	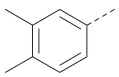	6.0	0.30	4.5	371	4.9
45	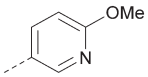	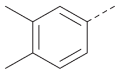	7.2	0.39	4.4	345	4.3
46		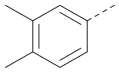	5.5	0.34	<4.5	305	3.3
47	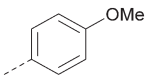	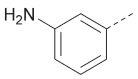	6.2	0.35	4.8	331	3.9
48	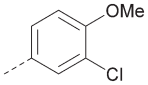		5.0	0.32	<4.3	315	4.2
49	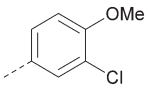	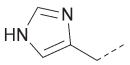	5.6	0.31	<4.8	355	3.9
50	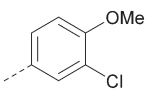	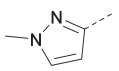	<5.0	NA	<4.5	355	4.3

Table 5 Target engagement and *in vitro* ADME data for selected compounds[c]

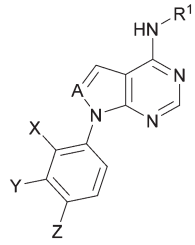

						Inhibition of PI5P4K (ADP-Glo)			Cellular target engagement (InCELL pulse)	*In vitro* ADMET[a]			
	R^1	X	Y	Z	A	PI5P4Kγ+ pIC_{50}	PI5P4Kβ pIC_{50}	PI5P4Kα pIC_{50}	PI5P4Kα pIC_{50}	P_{app} (A2B, 10^{-6} cm s^{-1})	ER	Solubility (μM)	MLM $t_{1/2}$ (min)
20	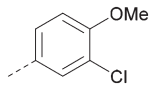	Me	H	Cl	N	<4.6	<4.6	6.6	6.4	6.4	0.7	10	26
ARUK2002821(**36**)	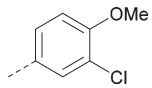	H	Me	Me	CH	<4.3	ND[b]	8.0	6.6	0.2	0.8	3	11
45	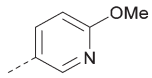	H	Me	Me	CH	<4.4	<4.6	7.2	<4.6	12	0.6	3	11
43	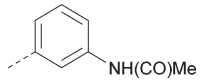	H	Me	Me	CH	<4.5	<4.6	6.8	5.7	14	0.9	3	24
39	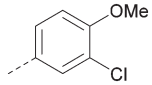	H	Me	Me	C(OH)	<4.6	ND	6.9	ND	17	0.7	1	16

[a] Experiments were performed at Cyprotex (see ESI†). P_{app} is apparent permeability and ER is efflux ratio, these were measured in MDCK-MDR1 cells. Solubility was determined at pH 7.4 in aqueous buffer. MLM $t_{1/2}$ is the half-life of compound when incubated with mouse liver microsomes. [b] **36** showed 4% inhibition when screened in this assay at a single concentration of 100 μM. [c] ND = not determined.

slightly less active than 3,4-dimethyl (compare **36** and **41**) and the 4-OMe matched pair with **8** also tracks well (**42**; Table 4). A primary aim was to improve molecular properties, particularly reducing lipophilicity. To this end, polar substituents and heteroaromatic rings were trialled in different positions for R^1 and R^2. Acetamide at the meta position (**43**) showed a marked drop in $X\log P$ compared to **36** but with a drop in activity and the para acetamide **44** showed a further drop in activity. Pyridyl derivative **45** showed a good balance of activity and $X\log P$, whereas isoxazole **46**, which had a favourable $X\log P$, lost considerable potency. At position R^2, a more polar aniline substituent was somewhat tolerated (**47**) whereas a small aliphatic group was again not tolerated (compare **48** and **29**), nor were 5-membered heterocycles in different configurations (**49**, **50**).

A set of compounds from this series spanning different cores and R^1 and R^2 groups that were beneficial for potency and/or favourably modified physicochemical properties was profiled in further assays including PI5P4K isoform selectivity, a PI5P4Kα cellular assay to demonstrate target engagement and simple ADMET assays including permeability, solubility and microsomal stability (Table 5). In general, compounds from this series did not inhibit PI5P4Kγ+ or PI5P4Kβ and were able to engage PI5P4Kα in cells as measured using an InCELL Pulse thermostabilisation assay (DiscoverX). These compounds displayed moderate permeability scores and showed no efflux flags in MDCK-MDR1 cells, although solubility was generally low. Stability in mouse liver microsomes was moderate to low (Table 5).

Compound **36** (ARUK2002821) was identified as a promising lead in this chemical series, with good potency, selectivity *vs.* PI5P4Kβ and PI5P4Kγ+ and active cellular target engagement. To assess wider kinase selectivity, **36** was profiled against 140 protein kinases and 15 lipid kinases. When **36** was tested at 1 μM in the lipid kinase screen the only target with <50% residual activity was PI5P4Kα (15.6%) and the considerable drop to the next most inhibited target indicated high specificity (SPHK2; 81.7% residual activity; Table S10†). In the protein kinase screen no targets were inhibited by >50% at 1 μM; the lowest residual activities observed were for ERK1 and JAK3 (62 and 63%, respectively; Table S11†). Full data are provided in the ESI.†

In order to solve a structure of a co-complex of PI5P4Kα with a ligand from this series, a truncated version of human PI5P4Kα was cloned into a bacterial expression vector. Using this approach, a PI5P4Kα protein construct comprising residues Asp35 to Thr406, with the region between residues 308–314 deleted, was successfully co-crystallised with **36** at a 2.1 Å resolution (Fig. 2, pdb 8C8C).

There is one PI5P4Kα chain in the asymmetric unit. This forms a dimer interface with a symmetry-related chain, which is similar to that seen in the published unliganded structure of PI5P4Kα (pdb 2YBX). Overall, the protein structure with **36** bound shows a high degree of similarity with that of the apo structure (Fig. 2A). However, the Lys228–Thr232 loop segment has a different orientation in the **36** complex, resulting in Leu230 becoming part of the binding pocket. In addition to the Lys228–Thr232 loop, four residues in the binding pocket are significantly re-oriented compared with apo structure 2YBX: Asn124, Phe134, Lys145 and Lys209 (Fig. 2B). The re-orientation of these residues upon ligand binding is also seen in several other crystal structures that have become available in the public domain since we solved this structure, *e.g.* pdb 6OSP and 6UX9.[19,21] The latter structures differ, though, in that they do not show the re-positioning of the 'activation loop' that results in Leu230 becoming part of the binding pocket. There are four regions of significant disorder

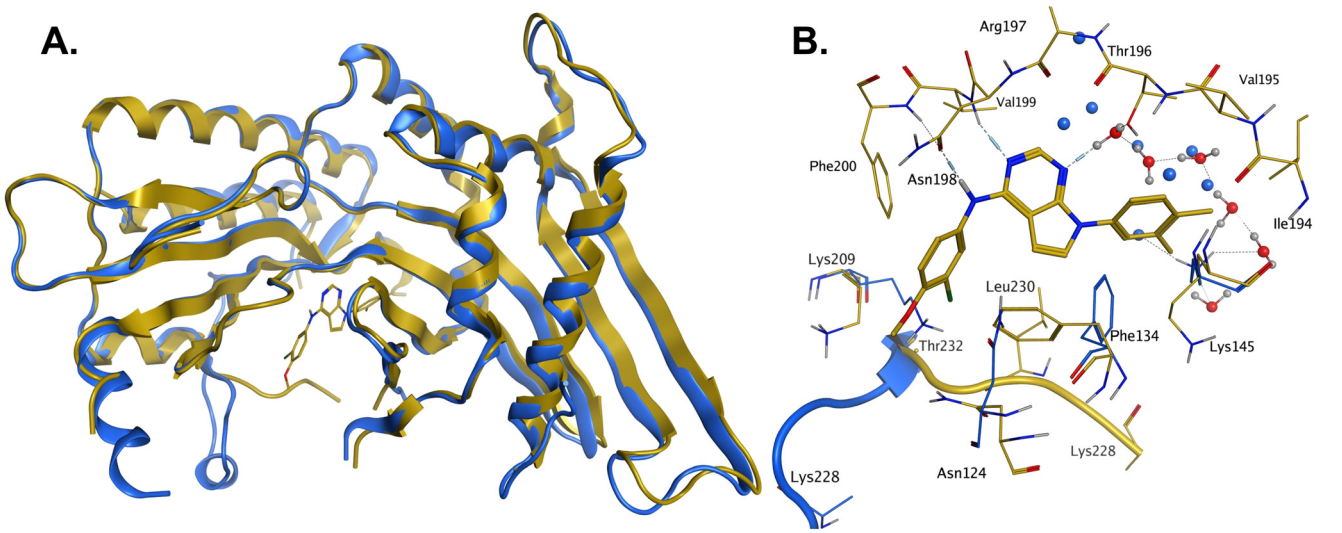

Fig. 2 A: Crystal structure comparison of apo PI5P4Kα (pdb 2YBX; blue) and PI5P4Kα in complex with compound **36** (pdb 8C8C; gold). B: View of the active site of PI5P4Kα in complex with compound **36** (gold carbons). Residues of the apo structure 2YBX that are in a different orientation in the ligand-bound structure are shown in blue, and the Lys228–Thr232 loop segment of the apo structure as a blue ribbon. 2YBX waters are shown as blue spheres, and 8C8C waters with red oxygen atoms.

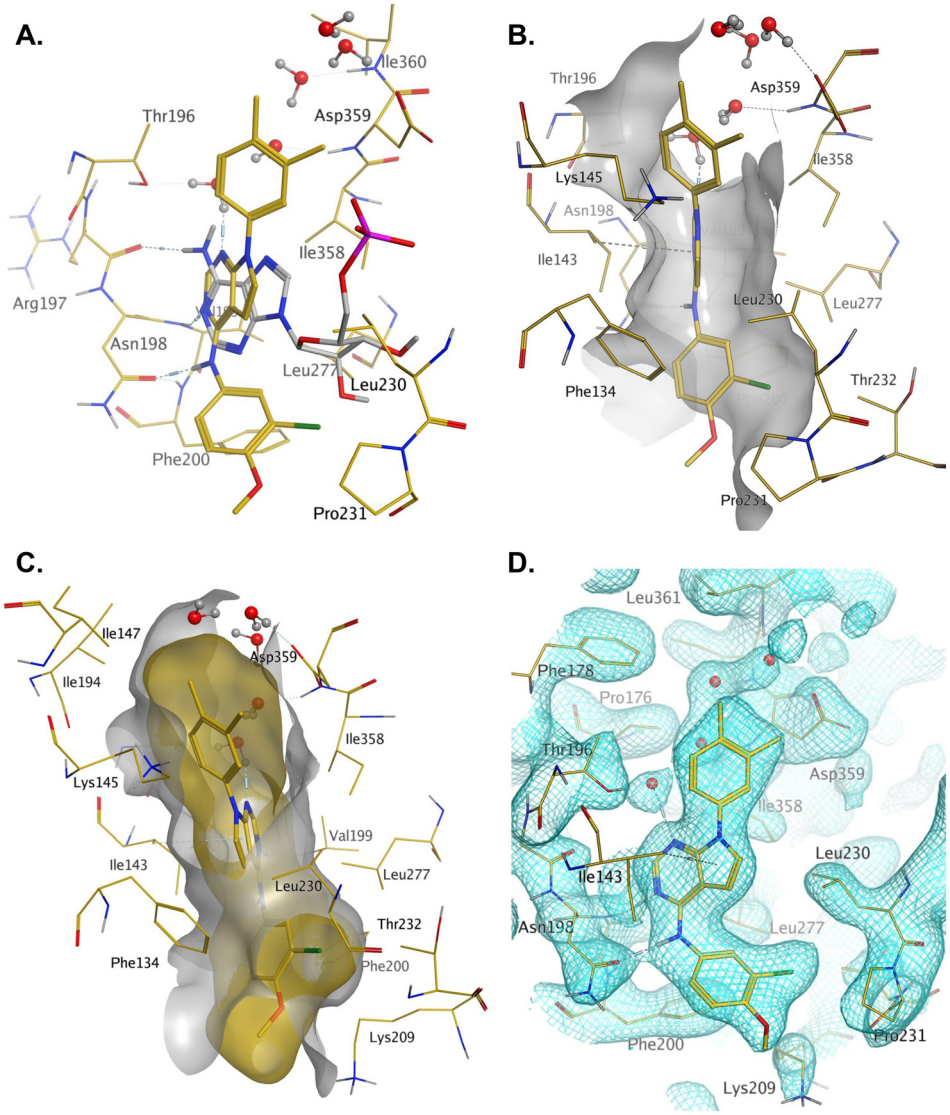

Fig. 3 A: AMP co-factor of PI5P4Kβ (3X01, grey) superposed onto chain A of the **36**–PI5P4Kα complex (pdb 8C8C, gold carbons); B: binding pocket in chain A of the **36**–PI5P4Kα highlighting the hydrophobic cleft; C: binding pocket of the **36**–PI5P4Kα complex with ligand and protein molecular surfaces; D: electron density at 1σ for protein residues and **36** in the binding pocket.

in the **36**-bound structure: loop regions Ser126–Ala132, Thr216–Ala227, Glu289–Pro336 and Lys369–Ser386.

Compound **36** binds to the same pocket occupied by AMP in the PI5P4Kβ crystal structure (pdb 3X01; Fig. 3A). The binding pockets of the PI5P4Kβ crystal structure and the **36**–PI5P4Kα structure are almost identical near the hinge, but the area where the sugar moiety binds in PI5P4Kβ is occupied by Leu230 in the **36**–PI5P4Kα complex. **36** binds deeply in the hydrophobic cleft that forms the ATP binding site in lipid kinases. In particular, the compound binds in the largely hydrophobic pocket formed by Phe134, Ile143, Phe200, Leu230, Leu277 and Ile358 (Fig. 3A and B). The NH linker in **36** forms a hydrogen bond with the side-chain oxygen acceptor of Asn198, while N1 (see heterocycle numbering in Table 3) of compound **36**'s pyrrolopyrimidine forms a hydrogen bond with the main-chain nitrogen of

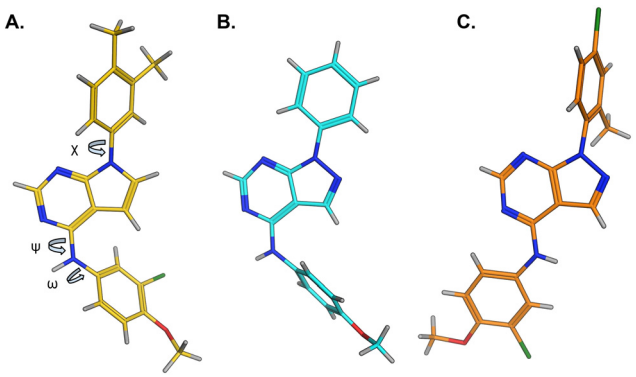

Fig. 4 A) Conformation of **36** as bound in complex with PI5P4Kα (pdb 8C8C); B) X-ray conformation of a related compound (CSD: ETUWAU); C) small molecule X-ray structure of compound **20** (CSD: 223787). Key dihedral angles are indicated with Greek letters.

Val199 (Fig. 2B). Furthermore, N3 of the pyrrolopyrimidine is seen to make a hydrogen bond interaction with an ordered water in the binding site. This water is positioned by further hydrogen bonding to the side-chain oxygen acceptor of Thr196 (Fig. 2B and 3A). This results in a repositioning of the water network at the top of the binding pocket, when compared with the apo structure 2YBX (Fig. 2B). As mentioned above, the side-chains of Phe134, Asn124, Lys145 and Lys209 have been re-orientated compared with the apo structure (Fig. 2B). These side-chain re-orientations result in a tight fit of the aniline aromatic ring, with the chlorine contacting the lipophilic part of the Lys209 and Thr232 side chains, as well as Leu230 and Leu277 (Fig. 3C). The methoxy group of **36** is solvent-accessible whereas the dimethylphenyl group partially fills a lipophilic pocket, with the remaining space of the pocket being occupied by a network of water molecules. The 4-methyl group makes contact with the side chains of Ile147, Ile194 and Lys145, whereas the 3-methyl group mainly interacts with Asp359. All atoms of the ligand are visible in the electron density (Fig. 3D).

Discussion and conclusions

The effects of the modifications to the bicyclic core (Table 3) are generally explained very well by the crystal structure of the **36**–PI5P4Kα complex. Both N1 and N3 are involved in hydrogen bonding, so changing either nitrogen to a carbon leads to loss of potency (**38** and **37** respectively, *vs.* **36**). N8, on the other hand, is in a very lipophilic environment created by the Leu230 and Phe134 side-chains. Therefore, substituting this nitrogen for a carbon increases potency (**26** *vs.* **36**). The C7 methyl substitution of **40** prevents the ligand from adopting the binding conformation, so leads to loss of potency. The importance of the *meta*-Cl substitution for potency, evident from the data in Tables 1 and 2, arises from the interaction with Leu230, Thr232 and Lys209 in a very lipophilic pocket just large enough to fit the chlorine atom (Fig. 3C). However, **32** and **35** are inactive despite having the R^1 *meta*-Cl substituent. QM calculations suggest that these ligands favour a conformation where R^1 and the pyrimidine core are in plane rather than at the 45° torsion angle (Fig. 4A: dihedral ω) seen for **36** in the complex. In this planar conformation the R^1 group has rotated 180° around the NH–pyrimidine bond (dihedral ψ), so that the NH is no longer available for hinge-binding (as in Fig. 4C). QM calculations indicate that ligands with electron-donating substituents on R^1 tend to favour the binding conformation seen for **36**, and those with electron-withdrawing substituents favour the planar conformation (Fig. 4C) due to increased conjugation between the ring systems. A small molecule crystal structure of **20** shows that this compound adopts a non-hinge-binding conformation in its crystal form, whereas a similar structure in the CSD without the chlorines adopts the hinge-binding conformation (CSD-ETUWAU;[29] Fig. 4B). It is likely that conformational preference for a particular ω angle also plays a role. *Ab initio* optimization of **36** in the bound conformation changed ω angle from −45 to −60 degrees. This optimized ligand still fits well in the binding site. However, starting from the crystal structure conformation, compounds **32** and **35** optimized to ω angles of −83 and −96 degrees, respectively, which results in a clash with Phe134 when placed back in the binding site (see ESI† page S50). It appears that R^1 requires a delicate balance between substituents that make hydrophobic contacts and those that support the binding conformation.

The R^2 SAR in Table 2 shows that a *para*-methyl substitution is favourable, and the 8C8C structure shows that this methyl group makes hydrophobic contacts with the side-chains of Ile147, Ile194 and Leu361 (Fig. 3). Other *para* substituents appear not to be tolerated, *e.g.* the *para* chlorine of **19** and CF_3 of **28**. Given that the *p*-Cl group is tolerated on R^2 of **20**, where there is also an *ortho* substituent on the ring, the issue with the *p*-Cl group is likely to be again one of conformation of the ligand. The torsion angle between the core and R^2 ring (Fig. 4A: dihedral χ) is 55° in **36** in complex with PI5P4Kα, while small molecule crystallography suggests that the lowest energy conformation for an unsubstituted phenyl at R^2 is in plane with the core ring system (CSD-ETUWAU, Fig. 4B). *Ortho* substitution creates a favourable twist, whereas electron withdrawing groups and ring nitrogen atoms increase conjugation and thereby make this twist less energetically favourable.

In summary, a new PI5P4Kα-selective chemotype has been identified through virtual screening and optimised *via* iterations of design and synthesis to provide potent tool molecules to further probe the biology of this important target. ARUK2002821 (**36**) is a potent PI5P4Kα inhibitor (pIC_{50} = 8.0) which is selective *vs.* PI5P4Kβ and PI5P4Kγ and engages the target, in cells, at sub-micromolar concentrations. ADMET data has been provided for this tool molecule and others in the series, as well as an X-ray structure solved with this molecule as a complex with its PI5P4Kα target, so that researchers in the field of PI5P4K biology may have useful tools for further investigation.

Experimental details

Biochemical assays

Assays to determine kinase activity of PI5P4Ks in the presence of inhibitors using an ADP-Glo assay (Promega) were performed as described previously.[28] Recombinant PI5P4K protein was prepared as described previously.[10] *E. coli* BL21(DE3) clones harbouring PI5P4Kα (*PIP4K2A*; UniGene 138363) or PI5P4Kβ (*PIP4K2B*; UniGene 171988), cloned into pGEX6P plasmid (Cytiva), were used to overexpress these proteins. Cultures were induced with 0.4 mM IPTG overnight and probe-sonicated in the presence of protease inhibitors. GST fusion protein was harvested using a GSTrap FF affinity column (Cytiva) and the GST tag removed *in situ* with 50 U of PreScission protease (Cytiva) for 4 h at 4 °C. The cleaved protein was further purified by size-exclusion chromatography (ÄKTA Pure, Cytiva). PI5P4Kγ+ protein (a

genetically modified chimera of PI5P4Kγ with a specific activity close to that of the active PI5P4Kα isoform[10]) was generated from a pGEX6P construct harbouring PIP4K2C (UniGene 6280511) with a number of PI5P4Kα-like mutations (insertion of three amino acids (QAR) at 139 plus an additional 11 amino acid mutations: S132L, E133P, S134N, E135D, G136S, D141G, G142A, E156T, N198G, E199G and D200E) using the same protein purification method. The protein purity was confirmed by sodium dodecyl sulfate–polyacrylamide gel electrophoresis, and the concentration was determined by colorimetric assay (Bio-Rad).

Binding of compounds to PI5P4Kα in intact cells was assessed using an InCELL Pulse thermal stabilisation assay (DiscoverX). PI5P4Kα (*PIP4K2A*; UniGene 138363) was cloned into the pICP vector (DiscoverX) to allow overexpression of the ePL-tagged target. Hek293 cells stably expressing ePL-tagged PI5P4Kα were incubated with 25 nl of test compound in 100% DMSO in a black skirted PCR plate for 60 minutes at 38 °C. After incubation for 3 minutes at 46 °C, followed by cooling for 3 minutes at room temperature, 12 μl of EA-3 reagent (prepared as per the manufactures guidelines) was added to each well. The plate was then incubated for 60 minutes in the dark prior to luminescence reading on a Pherastar FSX plate reader (BMG Labtech).

Data analysis

Statistical analysis was performed using nonparametric testing in Prism 8 (GraphPad). Activity pIC_{50} values and *in vivo* binding pEC_{50} values were estimated using a 4-parameter fit (Dotmatics).

X-ray crystallography and structure determination

Crystallography was performed by Peak Proteins Ltd. Truncated human PI5P4Kα was expressed in *E.coli* BL21(DE3) Gold using a pET28b vector. Expression was induced using 0.1 mM IPTG and the cells cultured at 18 °C for 16 h before harvesting by centrifugation. The protein comprised of residues Asp35 to Thr406 with the region between residues 308–314 deleted. Purification of TEV-cleaved protein was by both affinity and size exclusion (Superdex 75) chromatography. The structure of the ligand complex was generated by co-crystallisation of human PI5P4Kα in the presence of **36**. Purified protein (12 mg ml^{-1}, 20 mM HEPES pH 7.5, 150 mM NaCl, 0.5 mM TCEP) was incubated with 3 mM **36** (from 100 mM stock in DMSO) for 1 hour at 4 °C. Crystals were grown by mixing protein in equal parts with 3% (w/v) PEG1000 3% (v/v) PEG600, 3% (v/v) PEG 500ME, 3% (v/v) PEG400, 40 mM calcium chloride, 40 mM sodium formate, 100 mM Tris–HCl pH 8.0 at 20 °C. For X-ray data collection they were flash-frozen and X-ray diffraction data were collected (I04 beamline, Diamond Light Source synchrotron facility, Oxford, UK) at 100 K. Data were processed using the XDS and Aimless software. The phase information necessary to determine and analyse the structure was obtained by molecular replacement (PHASER, CCP4) using the previously solved structure of a human PI5P4Kα (pdb 2YBX) as the search model. Subsequent model building and refinement was performed according to standard protocols with the software packages CCP4 and COOT. TLS refinement (REFMAC5, CCP4) has been carried out, which resulted in lower R-factors and higher quality of the electron density map. The ligand parameterisation and the generation of the corresponding library files was carried out with ACEDRG (CCP4). The water model was built with the "Find waters"-algorithm of COOT by putting water molecules in peaks of the F_o–F_c map contoured at 3.0σ followed by refinement with REFMAC5 and checking all waters with the validation tool of COOT. The criteria for the list of suspicious waters were: B-factor greater 80 $Å^2$, $2F_o$–F_c map less than 1.2σ, distance to closest contact less than 2.3 Å or more than 3.5 Å. The suspicious water molecules and those in the active site (distance to inhibitor less than 10 Å) were checked manually. The occupancy of side chains, which were in negative peaks in the F_o–F_c map (contoured at −3.0σ), were set to zero and subsequently to 0.5 if a positive peak occurred after the next refinement cycle. Parameterisation and the generation of the corresponding library files was carried out with ACEDRG (CCP4).

The Ramachandran Plot of the final model shows 96.5% of all residues in the most favoured region, 3.3% in the additionally allowed region. Statistics of the final structure and the refinement process are listed in Table S12.†

Computational modelling

The virtual screening procedure was performed as previously described.[25]

QM energy calculations were carried out with Jaguar (release 2016-3, Schrodinger, **https://www.schrodinger.com**). The structures were optimised at the M06-2X/cc-pVTZ(-f) theory level in solution (water : PBF) starting from both the **36** crystal complex conformation and the small molecule **20** crystal structure, and energies of the two resulting conformations for the same ligand were then compared.

Abbreviations

ATP	Adenosine triphosphate
LE	Ligand efficiency
LLE	Lipophilic ligand efficiency
MLM	Mouse liver microsomes
PI5P4K	Phosphatidylinositol 5-phosphate 4-kinase
QM	Quantum mechanics
SAR	Structure–activity relationship
WT	Wild-type

Author contributions

The manuscript was written through contributions of all authors. All authors have given approval to the final version of the manuscript. Stephen Andrews and Jonathan Clarke

were programme leaders, John Skidmore offered further project leadership; together all three designed the project plan. Henriëtte Willems developed the virtual screening workflow, selected VS hits and analogues for purchasing and docked compounds. Simon Edwards designed and synthesised the compounds. Helen Boffey and Stephen Chawner conducted studies with imanixil. Christopher Green and Tamara Romero developed the InCELL Pulse assay for PI5P4Kα. David Winpenny and Christopher Green ran ADP-Glo and InCELL Pulse assays and screened the compounds. Tamara Romero produced recombinant PI5P4K protein.

Conflicts of interest

There is no conflict of interest to declare.

Acknowledgements

This work was funded by Alzheimer's Research UK (grant: ARUK-2015DDI-CAM), with support from the ALBORADA Trust. The ALBORADA Drug Discovery Institute is core funded by Alzheimer's Research UK (registered charity no. 1077089 and SC042474). The authors wish to thank Professor David C. Rubinsztein for insightful discussions on the PI5P4K biology.

References

1 T. Balla, *Physiol. Rev.*, 2013, **93**, 1019–1137.
2 M. Chen, T. Wen, H. T. Horn, V. K. Chandrahas, N. Thapa, S. Choi, V. L. Cryns and R. A. Anderson, *Cell Cycle*, 2020, **19**, 268–289.
3 L. Palamiuc, A. Ravi and B. M. Emerling, *FEBS J.*, 2020, **287**, 222–238.
4 R. C. Wills and G. R. V. Hammond, *Biochem. J.*, 2022, **479**, 2311–2325.
5 J. E. Burke, *Mol. Cell*, 2018, **71**, 653–673.
6 J. R. Halstead, K. Jalink and N. Divecha, *Trends Pharmacol. Sci.*, 2005, **26**, 654–660.
7 F. M. Menzies, A. Fleming, A. Caricasole, C. F. Bento, S. P. Andrews, A. Ashkenazi, J. Füllgrabe, A. Jackson, M. J. Sanchez, C. Karabiyik, F. Licitra, A. L. Ramirez, M. Pavel, C. Puri, M. Renna, T. Ricketts, L. Schlotawa, M. Vicinanza, H. Won, Y. Zhu, J. Skidmore and D. C. Rubinsztein, *Neuron*, 2017, **93**, 1015–1034.
8 N. Thapa, X. Tan, S. Choi, P. F. Lambert, A. C. Rapraeger and R. A. Anderson, *Trends Cancer*, 2016, **2**, 378–390.
9 G. K. Arora, L. Palamiuc and B. M. Emerling, *FEBS Lett.*, 2022, **596**, 3–16.
10 J. H. Clarke and R. F. Irvine, *Biochem. J.*, 2013, **454**, 49–57.
11 R. Fiume, Y. Stijf-Bultsma, Z. H. Shah, W. J. Keune, D. R. Jones, J. G. Jude and N. Divecha, *Biochim. Biophys. Acta, Mol. Cell Biol. Lipids*, 2015, **1851**, 898–910.
12 B. M. Emerling, J. B. Hurov, G. Poulogiannis, K. S. Tsukazawa, R. Choo-Wing, G. M. Wulf, E. L. Bell, H. S. Shim, K. A. Lamia, L. E. Rameh, G. Bellinger, A. T. Sasaki, J. M. Asara, X. Yuan, A. Bullock, G. M. Denicola, J. Song, V. Brown, S. Signoretti and L. C. Cantley, *Cell*, 2013, **155**, 844–857.
13 S. Chen, C. C. Tjin, X. Gao, Y. Xue, H. Jiao, R. Zhang, M. Wu, Z. He, J. Ellman and Y. Ha, *Proc. Natl. Acad. Sci. U. S. A.*, 2021, **118**, e2002486118.
14 J. G. Jude, G. J. Spencer, X. Huang, T. D. D. Somerville, D. R. Jones, N. Divecha and T. C. P. Somervaille, *Oncogene*, 2015, **34**, 1253–1262.
15 K. Lima, J. L. Coelho-Silva, G. S. Kinker, D. A. Pereira-Martins, F. Traina, P. A. C. M. Fernandes, R. P. Markus, A. R. Lucena-Araujo and J. A. Machado-Neto, *Cancer Genet.*, 2019, **233–234**, 56–66.
16 S. Zhang, Z. Li, X. Yan, L. Bao, Y. Deng, F. Zeng, P. Wang, J. Zhu, D. Yin, F. Liao, X. Zhou, D. Zhang, X. Xia, H. Wang, X. Yang, W. Zhang, H. Gao, W. Zhang, L. Yang, Q. Hou, H. Xu, Y. Zhang, Y. Shu and Y. Wang, *Front. Genet.*, 2019, **9**, 721.
17 K. A. Hinchliffe, R. F. Irvine and N. Divecha, *EMBO J.*, 1996, **15**, 6516–6524.
18 M. Kitagawa, P. J. Liao, K. H. Lee, J. Wong, S. C. Shang, N. Minami, O. Sampetrean, H. Saya, D. Lingyun, N. Prabhu, G. K. Diam, R. Sobota, A. Larsson, P. Nordlund, F. McCormick, S. Ghosh, D. M. Epstein, B. W. Dymock and S. H. Lee, *Nat. Commun.*, 2017, **8**, 2200.
19 S. C. Sivakumaren, H. Shim, T. Zhang, F. M. Ferguson, M. R. Lundquist, C. M. Browne, H. S. Seo, M. N. Paddock, T. D. Manz, B. Jiang, M. F. Hao, P. Krishnan, D. G. Wang, T. J. Yang, N. P. Kwiatkowski, S. B. Ficarro, J. M. Cunningham, J. A. Marto, S. Dhe-Paganon, L. C. Cantley and N. S. Gray, *Cell Chem. Biol.*, 2020, **27**, 525–537.e6.
20 T. D. Manz, S. C. Sivakumaren, A. Yasgar, M. D. Hall, M. I. Davis, H. S. Seo, J. D. Card, S. B. Ficarro, H. Shim, J. A. Marto, S. Dhe-Paganon, A. T. Sasaki, M. B. Boxer, A. Simeonov, L. C. Cantley, M. Shen, T. Zhang, F. M. Ferguson and N. S. Gray, *ACS Med. Chem. Lett.*, 2020, **11**, 346–352.
21 T. D. Manz, S. C. Sivakumaren, F. M. Ferguson, T. Zhang, A. Yasgar, H. S. Seo, S. B. Ficarro, J. D. Card, H. Shim, C. V. Miduturu, A. Simeonov, M. Shen, J. A. Marto, S. Dhe-Paganon, M. D. Hall, L. C. Cantley and N. S. Gray, *J. Med. Chem.*, 2020, **63**, 4880–4895.
22 K. Lima, D. A. Pereira-Martins, L. B. L. de Miranda, J. L. Coelho-Silva, G. da S. Leandro, I. Weinhäuser, R. de C. Cavaglieri, A. de M. Leal, W. F. da Silva, A. P. A. de L. Lange, E. D. R. P. Velloso, E. Griessinger, J. R. Hilberink, E. Ammatuna, G. Huls, J. J. Schuringa, E. M. Rego and J. A. Machado-Neto, *Blood Cancer J.*, 2022, **12**, 151.
23 M. I. Davis, A. T. Sasaki, M. Shen, B. M. Emerling, N. Thorne, S. Michael, R. Pragani, M. Boxer, K. Sumita, K. Takeuchi, D. S. Auld, Z. Li, L. C. Cantley and A. Simeonov, *PLoS One*, 2013, **8**, e54127.
24 N. J. Sumi, B. M. Kuenzi, C. E. Knezevic, L. L. Remsing Rix and U. Rix, *ACS Chem. Biol.*, 2015, **10**, 2680–2686.
25 T. P. C. Rooney, G. G. Aldred, H. K. Boffey, H. M. G. Willems, S. Edwards, S. J. Chawner, D. E. Scott, C. Green, D. Winpenny, J. Skidmore, J. H. Clarke and S. P. Andrews, *J. Med. Chem.*, 2023, **66**, 804–821.
26 L. Wortmann, N. Bräuer, S. J. Holton, H. Irlbacher, J. Weiske, C. Lechner, R. Meier, J. Karén, C. B. Siöberg, V. Pütter, C. D. Christ, A. ter Laak, P. Lienau, R. Lesche, B.

Nicke, S. H. Cheung, M. Bauser, A. Haegebarth, F. von Nussbaum, D. Mumberg and C. Lemos, *J. Med. Chem.*, 2021, **64**, 15883–15911.

27 M. D. Voss, W. Czechtizky, Z. Li, C. Rudolph, S. Petry, H. Brummerhop, T. Langer, A. Schiffer and H. L. Schaefer, *Biochem. Biophys. Res. Commun.*, 2014, **449**, 327–331.

28 H. K. Boffey, T. P. C. Rooney, H. M. G. Willems, S. Edwards, C. Green, T. Howard, D. Ogg, T. Romero, D. E. Scott, D. Winpenny, J. Duce, J. Skidmore, J. H. Clarke and S. P. Andrews, *J. Med. Chem.*, 2022, **65**, 3359–3370.

29 A. Al-Azmi, *Curr. Org. Chem.*, 2020, **24**, 216–229.